JOURNAL OF GEOPHYSICAL RESEARCH, VOL. 113, A09310, doi:10.1029/2007JA012781, 2008

Estimating the daytime Equatorial Ionization Anomaly strength from electric field proxies

C. Stolle,[1] C. Manoj,[2,3] H. Lühr,[1] S. Maus,[2] and P. Alken[2]

Received 30 August 2007; revised 28 March 2008; accepted 11 April 2008; published 10 September 2008.

[1] The Equatorial Ionization Anomaly (EIA) is a significant feature of the low-latitude ionosphere. During daytime, the eastward electric field drives a vertical plasma fountain at the magnetic equator creating the EIA. Since the eastward electric field is also the driving force for the Equatorial Electrojet (EEJ), the latter is positively correlated with the EIA strength. We investigate the correlation between the zonal electric field and the EIA in the Peruvian sector and compare the results with correlations of the EEJ versus EIA strength. Analyzing 5 years of Challenging Minisatellite Payload (CHAMP) electron density measurements, plasma drift readings from the Jicamarca Unattended Long-term Investigations of the Ionosphere and Atmosphere (JULIA) radar, and magnetic field observations at Huancayo and Piura, we find the EEJ strength and the zonal electric field to be suitable proxies for the EIA intensity. Both analyses reveal high correlation coefficients of $cc > 0.8$. A typical response time of the EIA to variations in the zonal electric field is $\sim$1–2 h, and it is $\sim$2–4 h after EEJ strength variations. Quantitative expressions are provided, which directly relate the EIA parameters to both proxies. From these relations, we infer that an EIA develops also during weak Counter Electrojets (CEJs), but no EIA forms when the vertical plasma drift is zero. For positive EEJ magnetic signatures to form, a minimum eastward electric field of 0.2 mV/m is required on average. The above-mentioned delay between EIA and EEJ variations of $\sim$3 h is further confirmed by the investigation of the EIA response to transitions from CEJ to EEJ, e.g., during late morning hours.

Citation: Stolle, C., C. Manoj, H. Lühr, S. Maus, and P. Alken (2008), Estimating the daytime Equatorial Ionization Anomaly strength from electric field proxies, *J. Geophys. Res.*, *113*, A09310, doi:10.1029/2007JA012781.

1. Introduction

[2] The Equatorial Ionization Anomaly (EIA) is a typical phenomenon of the *F* region ionosphere at low latitudes. It is characterized by an electron density trough at the magnetic dip equator, and a dual band of enhanced electron density at about 15° north and south of the trough. The EIA was discovered by *Appleton* [1954] and it has repeatedly been reviewed in the literature [e.g., *Anderson*, 1981; *Stenning*, 1992; *Walker et al.*, 1994]. The formation of the EIA is a result of the diurnal variation of the zonal electric field, which primarily points eastward during the day. With the horizontal geomagnetic field at equatorial latitudes, the plasma is lifted up by vertical $E \times B$ drift. Once transported to higher altitudes, the plasma diffuses downward along the geomagnetic field lines into both hemispheres due to gravitational and pressure gradient forces. The overall process is known as the ''fountain effect'' [*Duncan*, 1959]. Understanding the mechanism that causes the build-up of the EIA is the first step for predicting many ionospheric processes at low latitudes. Therefore the EIA, which is subject to considerable day-to-day variability, is a crucial challenge in sophisticated models of the upper atmosphere [e.g., *Millward et al.*, 2001; *Namgaladze et al.*, 1991; *Richmond et al.*, 1992; *Schunk et al.*, 2005].

[3] The daytime electric field is primarily controlled by the E region dynamo [*Heelis*, 2004], which is the driving force for both the vertical plasma drift and the Equatorial Electrojet (EEJ), in addition the EEJ strength is influenced by the E region conductivity [*Kelley*, 1989, pp. 86]. This is not the case for the vertical plasma drift. However, in search for a suitable proxy reflecting the EIA strength, a number of studies have been devoted to investigate the relation between the daytime E region currents and the structure of electron density distribution at low latitudes. *Dunford* [1967] showed experimentally for the first time a positive correlation between these quantities. In his study, he related electron density observations at 450 km obtained by the Alouette 1 topside sounder with daily variations of the horizontal component of hourly geomagnetic field data from four Indian observatories. On the basis of Total Electron Content (TEC) data over India, *Deshpande et al.* [1977] showed a strong EIA on a day with strong Equatorial Electrojet (EEJ), a short-lived EIA on a day with a Counter Electrojet (CEJ) in the afternoon, and the absence of the EIA on a day when no electrojet developed. They proposed a response time of the anomaly crest to changes in the E-layer

[1]GFZ German Research Centre for Geosciences, Potsdam, Germany.
[2]CIRES, University of Colorado and NOAA's National Geophysical Data Center, Boulder, Colorado, USA.
[3]National Geophysical Research Institute, Hyderabad, India.

0148-0227/08/2007JA012781$09.00

dynamics of 2–3 h. *Abdu et al.* [1990] compared the height of the F2-layer peak in the trough region with the strength of the EEJ at Brazilian longitudes for days in September/October 1986. They reported an excellent positive correlation between layer height and EEJ strength both for local time and day-to-day variation. A decorrelation occurs after 16:00–17:00 LT. The authors found response times of 2.5 to 4 h between the F2-layer peak height at the equator and the enhanced magnitude of the electron density at crest latitudes. The response time was suggested to depend on the vertical drift velocity, the height of the populated flux tube (longer plasma diffusion time from the equator to crest latitudes for higher flux tubes), and on the intensity of meridional winds. *Huang et al.* [1989] correlated the EIA parameters, crest magnitude and crest latitude, both derived from low-latitude TEC observations, with the maximum EEJ strength of the respective day. They found correlation coefficients, $cc = 0.53\ldots0.68$, for the crest latitude, and lower, $cc = 0.26\ldots0.37$, for the crest magnitude. They concluded that the electron density distribution is more directly affected by the E-field than the peak electron density. *Huang et al.* [1989] found also a seasonal dependence of the correlation between EEJ and crest latitude which they attributed to seasonal variation in the neutral wind system. *Rastogi and Klobuchar* [1990] correlated the ratio of TEC from crest stations and equatorial stations at 14:00 LT with the EEJ strength at 11:00 LT during 1975 and 1976. They found an approximately linear dependence between the TEC ratio and the EEJ strength. The relation is further enhanced when considering the mean EEJ strength between 7:00 and 14:00 LT. The authors observed that magnetic activity has a minor influence on the extent of the EIA but it is directly controlled by the EEJ strength. Further support for this relation comes from *Rama Rao et al.* [2006]. They correlated the daily summed electrojet strength with the EIA crest amplitude ($cc = 0.62$) and latitude ($cc = 0.72$) using TEC data from 38 days during solar minimum.

[4] *Su et al.* [1995] investigated the influence of vertical plasma drift on the electron density structure in the upper *F* region. They applied in situ electron density measurements at 600-km altitude from the Hinotori satellite to build a mean distribution of low-latitude electron density over local time. These data originate from high solar and low magnetic activity spanning the period November 1981 to February 1982. *Su et al.* [1995] then compared outputs from an ionospheric model with their empirical map. A good model for vertical plasma drift was identified to be the most important ingredient to satisfy the ionospheric observations.

[5] As pointed out here, a number of correlation studies between the EEJ strength and low-latitude ionospheric electron content have been presented so far. To our knowledge, no paper exists which also examines the relation between the EIA and a direct estimate of the eastward electric field, such as from vertical plasma drift observations, in a statistical manner. In this paper, we compare vertical plasma drift observations from the JULIA radar at the Jicamarca observatory site with the *F* region electron density distribution obtained from in situ measurements onboard the Challenging Minisatellite Payload (CHAMP) satellite and discuss the following questions: To what extent is the electric field correlated with the EIA? Are these results different from correlations with the EEJ strength? Addressing these issues provides new insights into the utility of the EEJ strength as a proxy for the EIA intensity.

2. Instrumentation and Data

2.1. CHAMP Satellite Observations

[6] The Challenging Minisatellite Payload (CHAMP) satellite was launched on 15 July 2000 into a near-circular, near-polar (inclination = 87.3°) orbit with an initial altitude of about 450 km which decayed to about 350 km in 2006 [*Reigber et al.*, 2002]. Successive satellite passes are separated by 23° in geographic longitude. The progress in local time is about 5.5 min per day, thus one full local time coverage is obtained in ~130 days. The instrument of particular interest for this study is the Planar Langmuir Probe (PLP). The PLP performs a 1-s sweep every 15 s to determine the in situ plasma density. There are almost continuous PLP observations available from 28 July 2000 up to date. The data we use are the Level 2 data products (CH-ME-2-PLP) accessible at GFZ's data center, ISDC (http://isdc.gfz-potsdam.de).

[7] The CHAMP PLP electron density readings have been validated by a comparison with plasma frequency measurements of the Jicamarca Digisonde [*McNamara et al.*, 2007]. Jicamarca is located at 11.95°S and −76.87°E (geographic), which is near the magnetic equator (~1°N (geomagnetic)) and the ionosonde therefore sounds primarily the EIA trough region. For CHAMP orbit heights below the F2 peak they report an average discrepancy between the PLP and ionosonde records of only 4%, with a standard deviation of 8.8%. At heights above the F2 peak a mean difference of 2.6% (standard deviation 13.3%) is given. Such discrepancies lie within the uncertainty of the ionosonde measurements and the applied electron density retrieval technique. In their study the CHAMP readings were found to be systematically lower than the ionosonde values.

[8] In Figure 1 the medium-thick lines (dashed, solid, and dash-dotted) show averages of latitudinal electron density profiles sampled along the CHAMP orbit at different heights. The curves are based on CHAMP observations from 934 days between 1 January 2001 and 31 December 2005. During that time the mean CHAMP orbital altitude decayed from 450 km to 350 km. Therefore the different height ranges reflect different mission periods. The height range above 410 km comprises observations between 1 January 2000 and 17 June 2003, the profile range between 410 km and 380 km includes observations between 31 August 2001 and 22 December 2004, and for the range below 380 km observations between 1 June 2004 and 31 December 2005 are available. All profiles show two local electron density maxima at about 15° north and south of the dip equator which occur when CHAMP crosses the crest regions. Because of orbit decay CHAMP samples different regions of the ionization anomaly over time. To obtain a consistent picture of the EIA structure, independent of sampling height, we decided to scale the PLP observations to a constant altitude of 400 km. For normalizing to a common height we employed the International Reference Ionosphere-2001 (IRI) model. For this purpose, we took the IRI prediction of electron density at the CHAMP measurement location (*IRI*(*in situ*)), and the prediction at the same location in longitude and latitude but at 400-km altitude

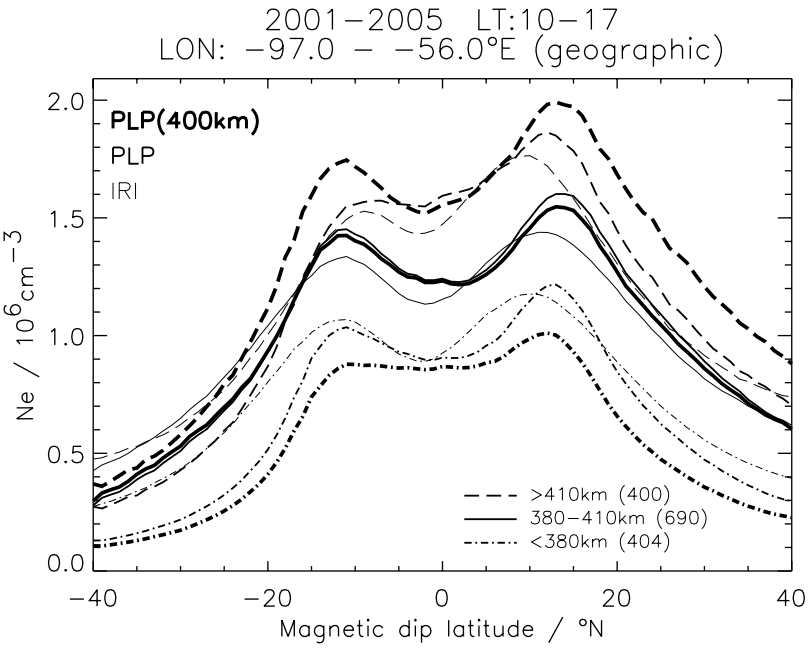

Figure 1. Average day side latitudinal electron density profiles (for $Kp < 3$), as derived from CHAMP PLP (PLP), as predicted by IRI (IRI), and from PLP readings normalized to 400-km altitude (PLP(400 km)). Sampled height ranges are given in the right bottom of the figure, where the total number of CHAMP orbits is also given in brackets.

(*IRI*(400 km)). Rescaling of each CHAMP measurement was then performed by the expression *PLP*(400 km) = *PLP*(*in situ*) · [*IRI*(400 km)/*IRI*(*in situ*)]. IRI provides the ionospheric climatology as monthly means [*Bilitza*, 1990]. The IRI electron density predictions have been found to agree reasonably well with the average PLP data on the dayside at low latitudes [*Liu et al.*, 2007]. The model still has shortcomings in predicting the postsunset EIA, but these times were not considered in our study. To illustrate the impact of the height correction, Figure 1 also shows average latitudinal profiles of the IRI and the scaled PLP data for different altitudes. An impression of the quality of the IRI predictions over the entire CHAMP mission can be obtained by comparing the medium-thick and thin lines in Figure 1. The IRI model outputs are slightly lower than the PLP measurements; however, the electron density profiles undergo similar changes between the different altitude ranges. The scaled PLP data (thick lines) from the highest altitude range show enhanced density peaks, almost no modification appears in the medium range around 400 km, and a flattening of the profile occurs for orbits below 380 km. One may have expected rather similar curves for the density profiles normalized to 400 km. However, the solar flux has a strong influence on the EIA. The differences between the three dashed curves are a consequence of the declining solar cycle during the CHAMP mission. The mean solar flux numbers are $F10.7 = 96$, 131, and 160 [$\cdot 10^{-22}$ W m^{-2} Hz^{-1}] from the lowest to the highest orbit range, respectively.

2.2. JULIA Radar Observations

[9] The Jicamarca Unattended Long-term Investigations of the Ionosphere and Atmosphere (JULIA) Mesosphere-Stratosphere-Troposphere (MST)/coherent scatter radar located at the Jicamarca Radio Observatory, Peru (see Figure 2) was designed for studying the day-to-day and long-term variability of equatorial irregularities. Its first observations, as well as a description of the instrument, were presented by *Hysell et al.* [1997]. The radar provides observations of so-called ''150-km echoes'' and the corresponding vertical Doppler velocity. By interpreting the latter quantity, *Kudeki and Fawcett* [1993] concluded that it reflects the vertical drift velocity of the ambient plasma, driven primarily by the zonal electric field component. The JULIA ''150-km echoes'' are recorded at a 5-min sampling period during daytime. Our analysis is based on 749 days of JULIA vertical drift data available between 1 August 2001 and 17 May 2006, rather uniformly distributed over the period. Coincidences with JULIA drift data were found for 487 CHAMP electron density profiles between 10:00 LT and 17:00 LT in the considered ±15° longitude sector around Jicamarca. The observations are distributed over 382 days. The justification for choosing this spatial range is given in section 3.1.

[10] Figure 3a shows the diurnal variation of the mean vertical plasma drift in 30-min averages as derived from all available JULIA ''150-km echoes.'' The number of measurements in each bin is also plotted. JULIA's best performance is around noon. A sufficient number of observations for statistical studies is available between 8:00 and 16:00 LT. The vertical plasma drift increases rapidly during the morning, achieving its maximum mean of ∼17 m/s between 10:00 and 11:00 LT. It is followed by a gradual decay to ∼8 m/s at 16:00 LT.

[11] When we compare the plasma drift with EIA observations, we automatically refer to the plasma drift pattern over a large ionospheric altitude range because the EIA is a result of plasma transport in all layers. Therefore let us briefly discuss the validity of the ''150-km echoes'' as an

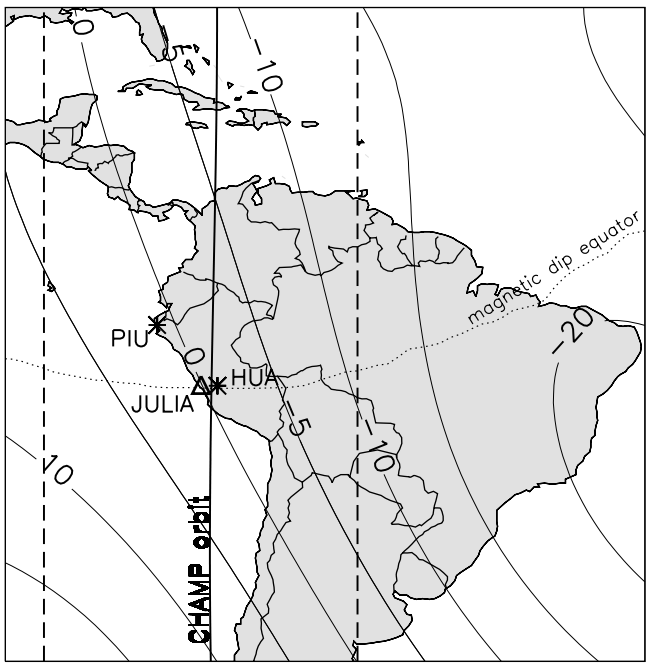

Figure 2. Plot of the measurement constellation. The triangle shows the location of the JULIA radar at Jicamarca. The asterisks mark the locations of the magnetometers Piura (PIU) and Huancayo (HUA). The thick solid vertical line gives the ground track of the CHAMP overflight on 10 October 2003 at ~19:45 UT (14:45 LT). The two vertical dashed lines are the borders of the area where CHAMP measurements are considered. The dotted lines give the magnetic dip equator as derived from CHAMP equatorial electrojet observations [*Lühr et al.*, 2004]. The declination isolines of the magnetic field, as derived from IGRF, are underlain (thin solid lines).

estimate of the F region electric field. It is known from theory that an altitude gradient of v_z, although very small, is crucial to satisfy the curl-free nature of the ionospheric electric field [*Murphy and Heelis*, 1986]. On the basis of incoherent scatter (IS) radar measurements, *Pingree and Fejer* [1987] found an increasing vertical velocity with height in the morning hours until 13:00 LT and a negative vertical velocity gradient in the afternoon, however, within only |0.05| m/s/km. Such small velocity gradients are confirmed by *Fejer et al.* [1995] who investigated the global F region vertical plasma drift based on AE-E satellite data. On the basis of an observed average daytime velocity $v_z \sim 20$ m/s, at all satellite altitudes (between 260 and 340 km), they suggested the absence of a significant height gradient in vertical drift on the dayside at F region altitudes. *Chau and Woodman* [2004] showed very good agreement between the daytime vertical Doppler velocities of "150-km echoes" and the mean F region drifts, with correlations of 0.93. They found the altitude gradient of vertical plasma drift to be nearly linear. The good agreement between drift estimates from "150-km echoes" and F region observations encourages us to rely on the JULIA observations as a general measure of the ionospheric vertical plasma drift.

[12] The local electric field ($\vec{E}$) perpendicular to an existing magnetic field ($\vec{B}$) is determined through the observed plasma drift velocity ($\vec{v}$) [*Kelley*, 1989, p. 68] by

$$\vec{E} = -\vec{v} \times \vec{B} \tag{1}$$

At equatorial latitudes, where the magnetic field is primarily directed northward, the observed vertical drift velocity provides an estimate of the eastward electric field. The International Geomagnetic Reference Field (IGRF) provides a magnetic field value at the Jicamarca site at 150-km altitude for 1 July 2003, which is the center of our analysis period, of B = 24,366 nT. Thus the variation of Δv_z = 1 m/s is caused by a $\Delta E_y = 24.4 \times 10^{-6}$ V/m, where E_y is the eastward electric field.

[13] The JULIA observation of vertical drift of ionospheric plasma can be highly variable over a day. In addition, there are frequent data gaps due to equipment malfunctioning. Therefore these data underwent a smoothing process before including them into our analyses. We applied a robust polynomial fitting to each day's diurnal variation and then estimated hourly means of the drift velocity centered on 8:30 LT through 15:30 LT with 1-h increments. We verified the diurnal variation of vertical drift individually for all days considered, to ensure that occasional disturbed data points did not influence the polynomial fit. To demonstrate our selection procedure, examples of diurnal observations of vertical plasma drift by JULIA and corresponding polynomial fits are presented in Figure 4. Days with a reliable polynomial data fit (e.g., 8, 10, and 17 October 2008) were considered for the comparison with CHAMP observations. (The two outliers above the line fit at about 8:30 LT and 13:00 LT at 8 October 2008 have been discarded to find the polynomial fit.) Noisy days like 13 October 2008 were fully rejected.

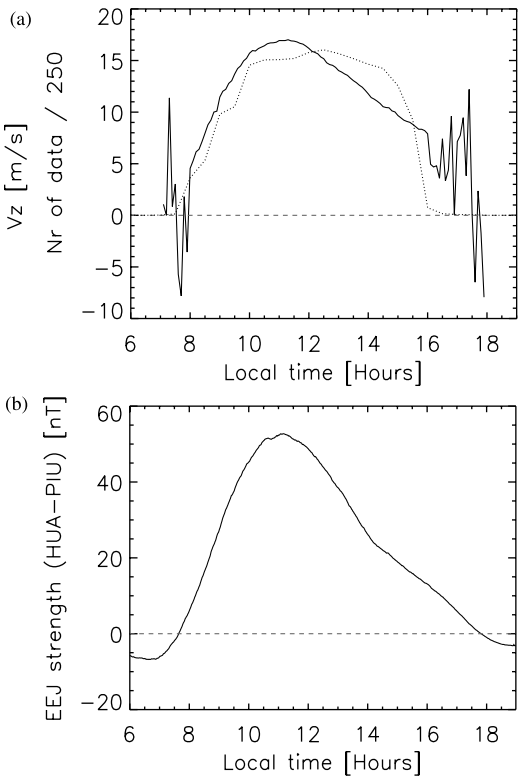

Figure 3. (a) Mean diurnal variation of JULIA vertical plasma drift (solid line) and considered number of data points (dotted line), as available between 2001.5 and 2005.5. The number of data points has been scaled down by 1/250 making it fit into the visualized frame. (b) Mean diurnal variation of the EEJ strength derived from the difference between Huancayo and Piura magnetic observations.

2.3. Observatory Magnetic Data

[14] For this study we also made use of the equatorial electrojet intensity. The EEJ current strength was computed from the horizontal intensities of the geomagnetic data observed at two low-latitude South American observatories Huancayo (HUA, 12.05°S, −75.33°E (geographic), −1.61° (geomagnetic)) and Piura (PIU 5.01°S, −81.07°E (geographic), 6.8° (geomagnetic), see Figure 2). For our study, we considered data sampled at 1-min interval during the time period of 2001 through 2005. Nighttime means were first subtracted from each data set. The residual magnetic field of PIU (ΔH_{PIU}) was subtracted from ΔH_{HUA} which is located within the EEJ footprint region. In this way we removed most of the nonionospheric magnetic signals from the HUA data. Thus, on a geomagnetically quiet day, the daily variation of the $\Delta H = \Delta H_{HUA} - \Delta H_{PIU}$ difference can reasonably well be used as a proxy for the EEJ current strength. For more details on the magnetic data processing see *Manoj et al.* [2006]. The average diurnal variation of the electrojet strength for the entire period of the study is presented in Figure 3b. In this longitude sector, the mean EEJ strength reaches a maximum of 53 nT, just before noon, at about 11:30 LT. The rising flank of the EEJ signal is steeper during the morning hours than during the afternoon decay.

[15] A total number of 1739 days of EEJ magnetic observations was available. For these days 1003 CHAMP electron density profiles between 10:00 LT and 17:00 LT within ±15° in geographic longitude around Jicamarca were identified to coincide with the EEJ measurements. These profiles are distributed over 788 days.

3. Ground-Satellite Correlation

3.1. Selection of Electron Density Profiles

[16] To conduct our study of the dayside ionosphere near Jicamarca we concentrated on electron density readings between January 2001 and June 2006. Because of the limitation in data availability, we had to use two slightly displaced 5-year study periods. For JULIA/CHAMP it ranges from 2001.5 to 2006.5 and for EEJ/CHAMP from 2001.0 to 2006.0. During each 5-year period, the CHAMP satellite covered all local time sectors 14 times, equally distributed over the seasons. No seasonal weighting is therefore needed in our analysis. The equal seasonal distribution helps, in particular, to obtain an average EIA structure which is very symmetrical about the dip equator because seasonal effects (caused, e.g., by meridional winds) compensate. The symmetry of the EIA shape is nicely recognized in Figure 1 for the averaged electron density profiles at all three height ranges.

[17] We selected CHAMP equatorial orbital segments, which cross the magnetic equator between 9:00 and

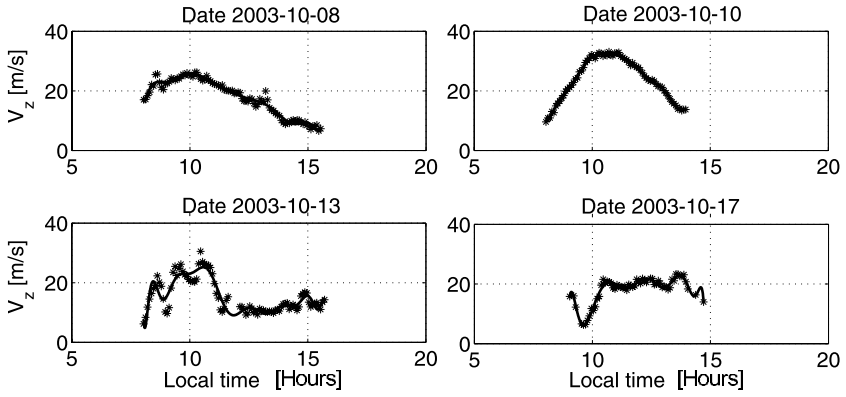

Figure 4. Examples of diurnal measurements of JULIA vertical drift (asterisks) and the polynomial fit applied to the observed time series (thick line).

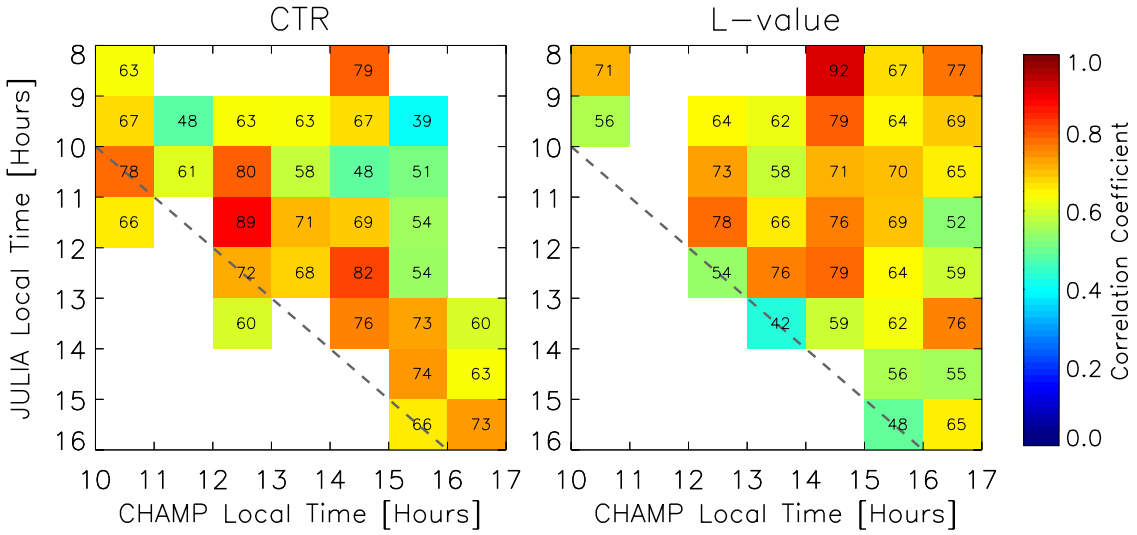

Figure 5. Correlation matrices for CTR and crest *L*-value versus vertical plasma drift. The number in each bin reflects the value of the correlation coefficient times 100. Insignificant correlation bins are blanked. The dashed line indicates simultaneous measurements without time delay.

17:00 LT, and between −91.8° and −61.8°E (geographic). The longitudinal range was chosen in accordance with results of *Manoj et al.* [2006] who found a ±15° correlation length of the equatorial electrojet. This 30° longitudinal sector is also well suited for a combined ground-satellite study of the EIA dynamics. As can be seen in Figure 2, CHAMP passes over the region strictly in a north-south direction. In addition, the zero-declination isoline crosses through Jicamarca, the center of the area. Therefore CHAMP tracks are well aligned with the local magnetic meridian, and nearly the same flux tube is sampled at the north and south EIA crests.

[18] CHAMP equator passes were considered here within a geographic latitudinal band of ±40° from the magnetic dip equator. After the data passed an integrity check, an automated detection algorithm was applied, which checks PLP measurements for typical EIA features. This process starts with low-pass filtered time series. The point of lowest electron density within a ±5° geographic latitude window about the dip equator was determined. Subsequently, we identified the global maxima north and south of this detected equatorial minimum. Only maxima exhibiting a curvature below a critical value were selected. If one maximum was accepted in each hemisphere, a trough point was identified. All profiles were checked individually for integrity of the identified extrema. The electron density readings at the two maxima ($\max_{north}$ and $\max_{south}$) and the minimum (min) from the unfiltered time series were stored together with their locations (geomagnetic latitude). Detected electron density maxima and minima were then used to derive characteristic EIA parameters from each profile, similar to equatorial TEC analyses [*Mendillo et al.*, 2000]. These are the Crest-to-Trough Ratio, $CTR = (\max_{north} + \max_{south})/(2 \cdot \min)$ and the *L*-value of the flux tube containing the electron density crest, $L = \frac{1}{2} \cdot (L_{north} + L_{south})$, as a measure of the EIA width. Here we have chosen the *L*-value to obtain an altitude-independent characteristic of the EIA. To compute the *L*-value, we assumed that the geomagnetic field can locally be approximated by dipole geometry. We thus get

$$L = \frac{r}{R_E} \frac{1}{\cos^2 \beta} \tag{2}$$

where r is the radial distance (measured in km) and β is the corrected magnetic latitude of the EIA crest observation, and R_E = 6371 km is the reference radius of the Earth [*Prölss*, 2005]. Since CTR is considered to be an important parameter, we concentrated on profiles with two detected maxima. Flat structures, similar to the corrected profile from heights below 380 km (see Figure 1), were included. Typical values of CTR, as derived from the CHAMP data for the analysis period, are $1 < CTR < 3.5$. If no anomaly is developed, this corresponds to $CTR = 1$. It was found that CTR experiences a significant day-to-day variability.

3.2. Method of Analysis

[19] The CHAMP electron density profiles sampled inside the ±15° longitude sector around JULIA were grouped into seven local time bins, 10 to 17 LT, with 1-h bin size. We allowed for a delayed response of the *F* region in determining the correlation between the electron density in the *F* region and the plasma drift in the E region. The CTR estimates in one LT bin were compared with all hourly means of the JULIA drift of that day (centered around 8:30 LT through 15:30 LT). This effectively creates a correlation matrix [number of CHAMP LT bins by number of JULIA LT bins]. The correlation coefficients between CTR estimates and JULIA drift were computed for each cell of the matrix, using a statistically robust procedure to ensure that a few bad data points did not influence the final result. Therefore a linear regression was first applied to the raw data set in each cell, determining the slope and intersect. Residuals of individual data points with respect to this line (initial guess) were calculated. Residuals were then sorted. Afterward, 10% of the data corresponding to the highest residuals were rejected. (10% is a trade off

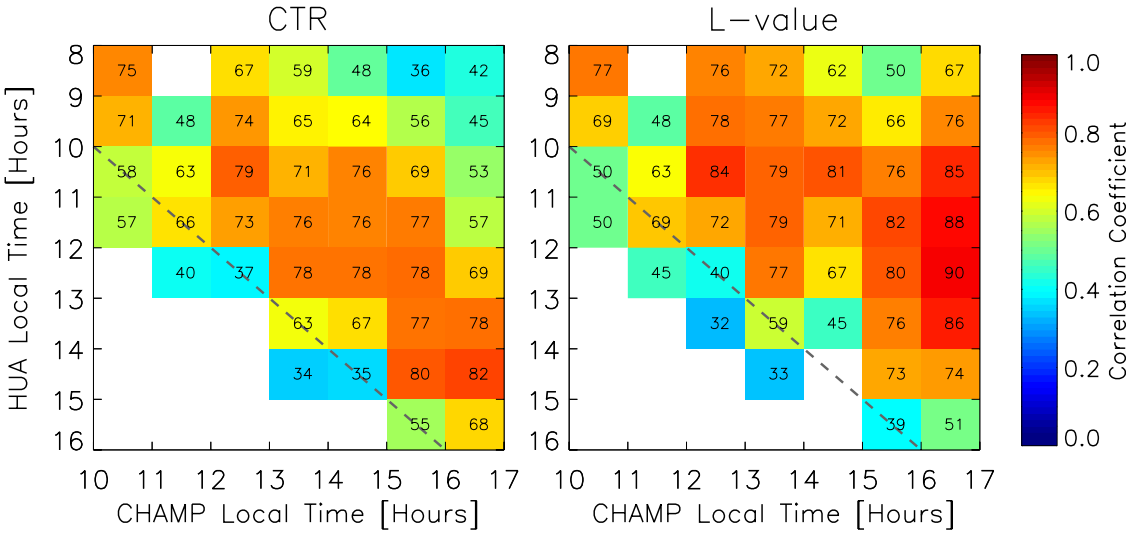

Figure 6. Correlation matrices for CTR and crest *L*-value versus magnetic EEJ observations. Otherwise as for Figure 5.

between number of data points and quality of the fit). A linear regression was performed again on the remaining data set to determine the correlation coefficient and slope parameters. The number of data points in the cells varied between 15 and 40, depending on the LT and lag parameters, and the majority of cells had 25 or more data pairs. The significance level for the correlation coefficients was computed by transforming the correlation to create a t-statistic having $N - 2$ degrees of freedom, where N is the number of data pairs in a particular local time bin. We kept correlation bins with a significance of correlation greater than 95%. The correlation analysis of the flux tube *L*-value versus v_z, and of CTR and *L*-value estimates versus the EEJ strength derived from magnetic data of $\Delta H_{HUA} - \Delta H_{PIU}$ were carried out separately in a similar fashion, using the same processing parameters as above. A complete description of the applied correlation process between ground and satellite data is given in *Manoj et al.* [2006].

[20] The data pairs were selected for magnetically quiet periods. For the correlation with v_z, we considered this condition as fulfilled when $Kp \leq 3$ held for 20–30 h before the equatorial pass. This preferred time delay of magnetic activity was based on a suggestion by *Scherliess and Fejer* [1997]. Using Jicamarca IS radar observations, they found the largest impact on the equatorial daytime vertical plasma drift (zonal E-field) for polar magnetic disturbances 20–30 h before the observation. We can confirm that using delayed *Kp* conditions results in a better correlation between the EIA and v_z rather then using instantaneous *Kp* or *Kp* delayed by 6 h. For correlation with the EEJ strength, only data were used when the instantaneous *Kp* value was below 3.

3.3. Correlation Results

3.3.1. Correlation of Vertical Drifts With Electron Density

[21] Figure 5 shows the matrices of correlations for CTR and crest *L*-values derived from CHAMP latitudinal profiles versus JULIA vertical drift measurements. The *x* axis gives the local time of the CHAMP equatorial passes and the *y* axis the local time of the drift hourly means. The correlation coefficients, *cc*, are represented by the color code and are typed as $cc \times 100$ into the respective bins. Blank bins indicate correlation results, which are not statistically significant at the 95% level. The dashed line follows correlation bins for ionospheric and electric field measurements taken at the same hour. To indicate correlation bins with 1-h delay between the two observation types, this line must be shifted upward by 1 h along the *y* axis, and respectively higher for longer delays.

[22] The highest correlation between CTR and v_z (see Figure 5, left) is found when we compare JULIA vertical drift measurements with CTR obtained 1 and 2 h later by CHAMP. This relation is manifested as a diagonal of high correlation in the matrix. We may calculate the mean correlation from bins with a fixed time delay (bins on lines parallel to the dashed diagonal line). The mean correlation is $cc = 0.72$ for zero time lag, but only 3 significant bins are available. The $cc = 0.72$ is true also for the 1-h delayed bins with significant values along the entire line, and the mean is also high for a 2-h delay with $cc = 0.69$. The correlation decreases significantly for CTR versus v_z delayed by 3 or more h.

[23] For correlations between the *L*-value and v_z (c.f. right panel in Figure 5) the mean correlation increases from $cc = 0.48$ for zero time lag to $cc = 0.65$ for the 1-h delayed bins but it peaks for the 2-h delayed bins ($cc = 0.68$). However, high correlation values are found in many places above the diagonal of the matrix.

3.3.2. Correlation of Electrojet Strength With Electron Density

[24] The correlation matrix for CTR versus EEJ strength is displayed in Figure 6 (left). The mean correlation increases from $cc = 0.52$ for zero time lag to $cc = 0.71$ for 1-h delays. The coefficients are highest for 2- and 3-h delays with $cc = 0.74$ and $cc = 0.75$. It returns to $cc = 0.71$ for 4 h, and *cc* decreases significantly for longer time delays.

[25] The correlation matrix of the crest *L*-value versus EEJ strength is presented in Figure 6 (right). Here we find an increase in the mean correlation from $cc = 0.51$ for zero time lag to $cc = 0.64$ along 1-h delay. The mean *cc* increases further with $cc = 0.72, 0.79, 0.81$ for delays of 2, 3, 4 h,

respectively. However, bins with high correlation are observed in the entire upper half of the matrix.

4. EIA Response to Counter Electrojet

[26] In the previous sections we have analyzed the correlation between the E region dynamics and the strength of the EIA. As a next step we investigate the response of the equatorial anomaly to a transient event. An obvious choice for that is the counter electrojet. The CEJ manifests itself by a negative excursion of the EEJ strength at equatorial stations [*Gouin and Mayaud*, 1967]. To identify a CEJ, we require a negative deflection below −5 nT lasting for at least 1 h. It is known that the CEJ occurs preferably during early morning (∼7:00 LT) and during afternoon hours ∼15:00 LT [e.g., *Rastogi*, 1974]. For that reason we have divided the identified events into two groups. For the first class the transition from CEJ to EEJ has to occur between 09:00 and 14:00 LT (i.e., $\Delta H_{HUA} - \Delta H_{PIU}$ has a positive slope and exceeds −5 nT). The second class is characterized by a transition from EEJ to CEJ taking place between 11:00 and 16:00 LT. For both classes, we identified about 50 events, which were accompanied by nearby CHAMP overflights.

[27] A superposed epoch analysis was applied to the EEJ strength separately for the two CEJ classes. In the first case the key time was the hour during which the EEJ strength switches from negative to positive and for the second class when it passed from positive to negative. In a superposed epoch analysis the time series of several events was synchronized by the key time and then averages over all events were calculated for each point in time. The average EEJ variations for the prenoon (58 cases) and the afternoon (40 cases) CEJs at HUA are presented in Figure 7.

[28] In the left column the temporal evolution of the EIA subsequent to a morning CEJ is shown. The superposed electron density profiles are normalized in amplitude in order to account for the day-to-day variability and to make them comparable. As expected, we find a single peaked density profile at 400-km altitude during the time of the counter electrojet. Only 2–3 h after the reversal in current direction, the double peaked ionization anomaly emerges. The bottom panel shows the average variation of the EEJ strength for the 10 h centered on the key time. A typical duration of the CEJ seems to be 5 h.

[29] An equivalent analysis, shown in the right column of Figure 7, was performed for the afternoon events. When starting at the top, we find the typical EIA profile before CEJ onset. After the reversal of current direction, the anomaly gradually decays and the EIA peaks are significantly reduced. The prominent density peak at northern latitudes in the frame 2–3 h after the CEJ onset is likely to be a seasonal effect, since all events contributing to these profiles were recorded in May or June. A double-peaked density profile emerges again after 5–6 h. This is just the time after which the average EEJ strength in the bottom frame recovers to positive values.

5. Discussion

[30] The aim of this study was to evaluate the suitability of the EEJ strength as a proxy for determining the EIA strength. To verify the results, we derived a similar relation between the E region vertical plasma drift (zonal electric field) and the EIA. As a test region, we chose the Peruvian sector, where suitable facilities (radar and magnetometer) are available close to the magnetic dip equator. The satellite CHAMP provided local *F* region electron density readings. This study covers new ground in considering, apart from the usual magnetic field derived EEJ strength, radar measurements of the zonal electric field. This study was carried out for dates covering a time span of 5 years. Special attention was paid to avoid local time and seasonal biases. Strictly speaking, our results are seasonally averaged and their validity is limited to the sector around the Peruvian sector. Because of the large-scale longitudinal variation of both the EEJ and the EIA, different relations are expected in other longitude sectors. In spite of that, our results can serve as a benchmark in future global studies.

5.1. Comparing EIA Correlations With v_z and EEJ Strength

5.1.1. Similarities

[31] We find highest mean correlation coefficients for the crest *L*-values at delay times 1 h longer than for correlations with CTR. The most favorable delays are 1 and 2 h when correlating v_z versus CTR and *L*-value, respectively, and 3 and 4 h when the EEJ strength is used. We suggest the following explanation for these observations: The equatorial ionospheric plasma is transported upward until it reaches the flux tube where density gradient and gravity forces are strong enough to stop the uplift process and forces the plasma to descend (and to move poleward) along the geomagnetic field lines. Therefore we expect that the magnitude of the EIA crests at 400 km, expressed by CTR, respond somewhat earlier than the width of the EIA. The latter response requires the entire time of plasma uplift and downward movement, while the CTR can peak already when the plasma is still at higher altitudes.

[32] Another similar feature between v_z and EEJ strength is the shorter correlation length in time for the CTR than for the *L*-value. Taking into account that the EIA peak electron density amplitude (considered for CTR) is also influenced by *F* region ionization and loss processes [e.g., *Huang et al.*, 1989], we expect a decorrelation with the E region electric field after a certain time. The width of the EIA (*L*-value) is mostly based on transport processes. Therefore longer correlation time lengths with the E region electric field are likely. These findings explain the higher correlation coefficients between the EEJ strength and *L*-value than that with CTR, as reported in earlier studies [e.g., *Dunford*, 1970; *Huang et al.*, 1989]. Especially when mean values or the daily summed EEJ strength are used for correlation with EIA parameters, improved results for crest width are found [*Rastogi and Klobuchar*, 1990; *Rama Rao et al.*, 2006].

5.1.2. Differences

[33] In this study we have used two different proxies for characterizing the zonal ionospheric electric field. One is the vertical plasma velocity at 150-km altitude, which is assumed to be governed by the large-scale $E \times B$ drift. The other is the magnetic deflection caused by the equatorial electrojet. The magnetic signature observed on ground

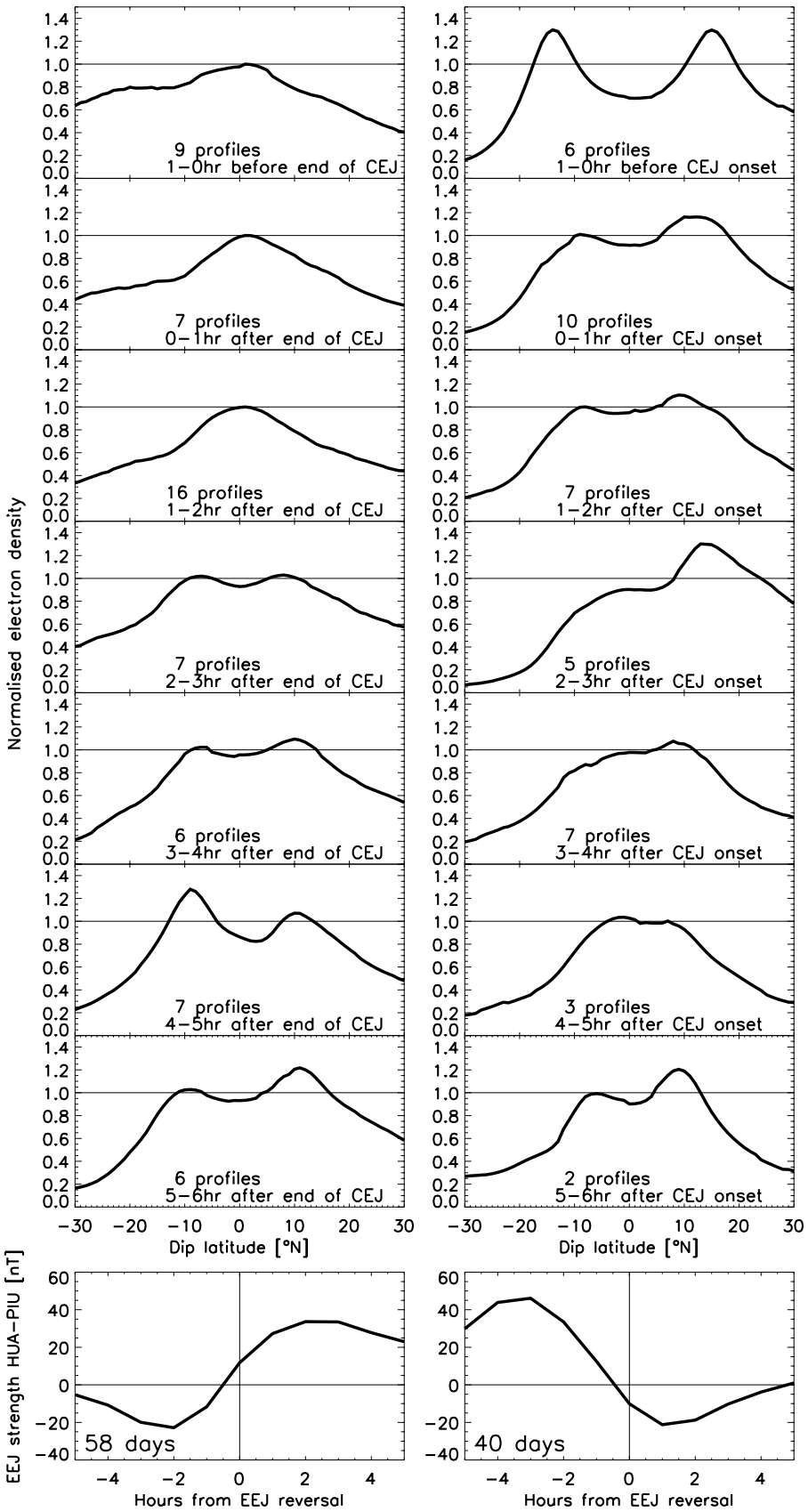

Figure 7. Average CHAMP electron density profiles before and after an EEJ current direction reversal. The number of involved profiles is indicated in each plot. Bottom: Averaged EEJ variations. Left: A change from CEJ to EEJ between 09:00 and 14:00 LT. Right: A turn from EEJ to CEJ between 11:00 and 16:00 LT.

Table 1. Correlation Coefficients Between P and the Quantities v_z at JULIA, HUA–PIU EEJ Strength, CTR, L-value, and Crest Density[a]

	JULIA v_z	EEJ Strength	CTR	L-value	Crest
cc	0.18	0.48	0.15	0.22	0.58
variation with P	+8.5%	+51.5%	+5.7%	+0.7%	+47.7%

[a]The lower row shows the relative increase of the quantities with P = 100–150 [$\cdot 10^{-22}$ W m^{-2} Hz^{-1}].

reflects well the height-integrated current density, $\vec{J}_{EEJ}$, of the EEJ. For that we can write

$$\vec{J}_{EEJ} = a_c \cdot \vec{E} \tag{3}$$

where a_c $\left(\text{in } \frac{\text{A}}{\text{Vm}}\right)$ is an effective conductivity and $\vec{E}\left(\text{in } \frac{\text{V}}{\text{m}}\right)$ is the eastward directed zonal electric field [*Prölss*, 2005]. It is well known that the conductivity depends on local time, solar EUV flux and on the presence of plasma instabilities. From this direct comparison one may conclude that the radar-based velocity measurements are preferable as a proxy for the E-field, over the magnetometer measurements. When looking at the correlation coefficients obtained through comparison with the vertical plasma drift velocity (v_z) and the EEJ strength in Figures 5 and 6, it is surprising to see that more significant and higher mean values of cc are obtained when using the EEJ strength, as compared to the vertical drift velocity from JULIA. As mentioned above, there is the conductance acting as the proportionally factor between EEJ current density and the E region electric field, which should reduce the correlation. However, obviously, the day-to-day variations of the conductivity are less prominent than those of the E-field. The somewhat lower correlation coefficients obtained with JULIA are probably caused by the very local nature of the radar velocity measurement. In contrast, ground-based magnetometer readings reflect the average ionospheric current density within a latitude range of about 100 km. This makes the EEJ data much smoother.

[34] In the previous section 5.1.1 we already mentioned that the best correlations of the EIA with the EEJ strength occur later than the best correlation of the EIA with v_z. The CTR versus v_z correlations peak at 1-h delays with cc = 0.72, and the CTR versus EEJ strength at 3-h delays with cc = 0.75. Similar results were found for L-value versus v_z, which peaks at 2-h delays with cc = 0.68 and L-value versus EEJ strength peaks at 4-h delays with cc = 0.81. As discussed above, the EEJ is a product of the eastward electric field and the conductivity, hence the EEJ magnetic signatures also include information on plasma density. The vertical plasma drift reflects the strength of the eastward electric field, unbiased by conductivity. We may conclude that the ionosphere responds to a certain ionospheric plasma drift pattern after a specific time, which is 1–2 h in our case. (Note, since JULIA v_z observations have been found to be highly correlated with F region drifts, our measurements contain information on the drift velocity over a wide ionospheric altitude range.) Correlations with the EEJ strength additionally consider the transport of the plasma from one place to another (since the EEJ is also determined by the amount of plasma through the plasma density contained in the conductivity term) and peak at a later time (3–4 h). A typical vertical plasma drift velocity is 20 m/s. During 3.5 h the plasma traverses a vertical distance of about 250 km.

5.2. Sensitivity of EIA on Electric Field Proxies

[35] In the previous section, we have seen that there are linear relations between the ionospheric E-field and some EIA parameters. Here we will focus on the scaling factors between the correlated quantities. The above-described correlations include the period of descending solar cycle 23 between 2001 and 2005. Before concentrating on the sensitivity analysis, we want to examine the sensitivity of the investigated quantities on solar flux. Table 1 reveals the correlation coefficient of mean daily JULIA v_z, daily mean EEJ strength, CTR, crest density, and L-value at 400-km altitude versus the solar activity proxy P = (F10.7 + F10.7A)/2 with F10.7A being the 81-day running mean of F10.7 centered on the day of interest. The table also gives the relative variation of the considered quantities for P between 100 and 150 [$\cdot 10^{-22}$ W m^{-2} Hz^{-1}], retrieved by linear regression analysis. For this analysis, v_z and EEJ magnetic observations were taken only from days, where CHAMP electron density profiles were available.

[36] A low correlation coefficient and only a moderate increase with P is observed for the daytime vertical plasma drift v_z. This finding confirms earlier satellite based observations of daytime F region v_z by *Fejer et al.* [1995], who even suggested that the daytime v_z is independent of solar activity. The vertical plasma drift is a measure of the equatorial zonal electric field which builds up in response to atmospheric tides (E-layer dynamo). Although still under investigation, a significant solar cycle dependence of neutral atmospheric tides is unlikely (J. Oberheide, personal communication, 2007). The situation changes for the EEJ strength with a significantly higher correlation and a dependence on solar activity. The conductivity plays an important role in controlling the EEJ strength. Since the conductivity is directly proportional to the charge density, a strong dependence on solar activity is expected. The table reveals that CTR and L-value are almost unaffected by solar activity variations. We may suggest that the daytime equatorial fountain is not (or only very weakly) P-dependent, as is the E-layer dynamo horizontal electric field. In comparison, the crest electron density is highly P-dependent.

[37] In the following we want to focus on EIA parameters measured 2 h after E-layer electric field readings which have been taken between 08:00 and 15:00 LT. To simultaneously investigate possible different effects, we chose a 2-h delay time, at which all correlations are high and can be considered as statistically significant. We further divided our database into four P-ranges of P = 70–100, 100–130, 130–160, and 160–190 [$\cdot 10^{-22}$ W m^{-2} Hz^{-1}]. Since our aim was to provide a reliable reference for EEJ strength analyses, we first examined correlations with v_z. For the first two solar activity levels, the CTR versus v_z correlation shows high coefficients of cc = 0.88 and cc = 0.82, respectively. These are cc = 0.93 and cc = 0.78 for L-value versus v_z. The lack of sufficient JULIA observations during high solar flux days may be the cause for the low coefficients of cc < 0.5 for the upper two P-ranges. To ensure reliable analyses based on significant results we concentrate in the following on low

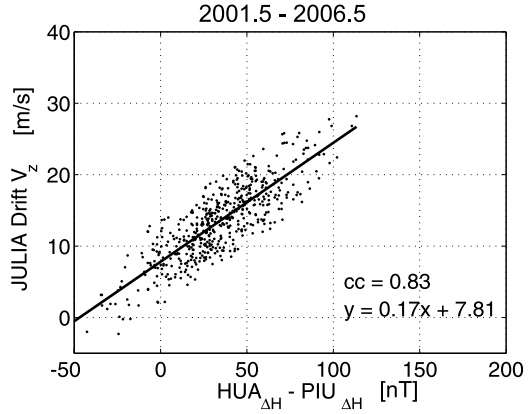

Figure 8. Daily range of ΔH versus the daily mean of JULIA plasma drift v_z. The correlation coefficient and regression line parameters are listed in the lower right.

solar flux conditions referring to $P = 70-130$. The regression lines from JULIA v_z correlations are

$$\begin{aligned} \mathrm{CTR} &= 1.01 + 44.8 \cdot 10^{-3} \frac{\mathrm{s}}{\mathrm{m}}\ v_z \\ &= 1.01 + 1.84 \frac{\mathrm{m}}{\mathrm{mV}}\ E_y \end{aligned} \tag{4}$$

$$\begin{aligned} L &= 1.081 + 1.97 \cdot 10^{-3} \frac{\mathrm{s}}{\mathrm{m}}\ v_z \\ &= 1.081 + 0.081 \frac{\mathrm{m}}{\mathrm{mV}}\ E_y \end{aligned} \tag{5}$$

$$\begin{aligned} h_{apex} &= 516\ \mathrm{km} + 12.5 \frac{\mathrm{km}}{\mathrm{ms}^{-1}}\ v_z \\ &= 516\ \mathrm{km} + 512 \frac{\mathrm{km}}{\mathrm{mV\ m}^{-1}}\ E_y \end{aligned} \tag{6}$$

where v_z is in units of m/s, E_y is the eastward electric field in mV/m, L is the L-value, and h_{apex} is the apex height in km of the flux tube containing the EIA crests. Here the result of (6) is derived from equation (5) by using $h_{apex} = R_E(L - 1)$. Equation (4) gives an intersect of almost 1, which means that a single peaked electron density profile is expected when no vertical drift is observed. Equation (6) gives an intersect of 516 km, which indicates that a clear EIA at satellite altitude (~400 km) is only discernable when the crest flux tube has reached a certain height.

[38] The corresponding regression analysis from EEJ strength correlations gives

$$\mathrm{CTR} = 1.39 + 9.7 \cdot 10^{-3} \frac{1}{\mathrm{nT}} \Delta H \tag{7}$$

$$L = 1.092 + 0.5 \cdot 10^{-3} \frac{1}{\mathrm{nT}} \Delta H \tag{8}$$

$$h_{apex} = 586\ \mathrm{km} + 3.2 \frac{\mathrm{km}}{\mathrm{nT}} \Delta H \tag{9}$$

with $\Delta H = \Delta H_{HUA} - \Delta H_{PIU}$ in units of nT. In equation (7) a bias value different from 1 emerges. This means that there is an additional background current that has to be taken into account. It also implies that the EIA can form even under weak counter electrojet conditions. The same is true if we consider equations (8) and (9) for the L-value of the crest and apex height which show significantly higher intersects than are found from correlations with the electric field in equations (5) and (6).

[39] We want to verify this relation by directly comparing the electric field and the EEJ strength. Figure 8 shows the result of correlating daily ranges of ΔH with daily means of simultaneous JULIA v_z. The figure includes all data available between 2001.5 and 2006.5. Here a robust correlation with 10% noise rejection was applied. This figure clearly shows that negative ΔH, corresponding to counter electrojet events, occur during upward plasma drift observations. A threshold vertical plasma drift velocity of ~8 m/s is derived from the linear regression corresponding to $E_y \sim 0.2$ mV/m. Independently, this threshold v_z can also be estimated when replacing the left-hand side of equation (4) with the intersect of equation (7) obtaining a very similar value of $v_z = 8.5$ m/s. This result is surprising, since the simple equation for J_{eej} (see equation (3)) requires an eastward electric field for an eastward EEJ. By correlating 10 days of EEJ strength observations with F region vertical plasma drifts obtained from Jicamarca IS radar observations, *Anderson et al.* [2002] retrieved linear relations between both quantities. They correlated two groups of events; when both the EEJ and v_z were positive or when both were negative. By this, they found a negative or positive intersect in v_z, respectively. Because of the restrictive selection of observations, these results are not directly comparable with our long-term data set. The investigation why a CEJ can be observed together with upward vertical plasma drift is beyond the scope of this paper. Here we want to point out that a positive bias value has to be taken into account when the EEJ strength is used as a proxy for EIA strength, at least in the Peruvian sector.

5.3. Reaction of EIA to Counter Electrojet

[40] Besides using statistical methods for studying the response of the EIA to E-layer dynamics we also looked at transient events. Here we focused on the occurrence of counter electrojets. In general, this additional analysis confirms the results of our statistical analysis.

[41] When looking at the morning events we find a single peaked density profile during and shortly after the CEJ. The suggested driver for this weak ion fountain is the electric field responsible for the background current. The EIA develops 2–3 h after the switch from CEJ to EEJ and it strengthens further. These observations are in excellent agreement with our statistical correlation results revealing a peak response time of 3 h.

[42] In the afternoon analyses we start with a well developed EIA before the transient event to CEJ. Shortly after the transition a reduction of the EIA profile occurs. However, it takes between 3 and 4 h until the electron density double peak vanishes. The decay of the EIA in response to the CEJ seems to last a little longer. It may take some extra time for the uplifted ions to diffuse down beyond the heights of the CHAMP orbit. However, at no time we do find a clear single peak, e.g., as was evident in early profiles from the morning analyses. Additionally, as soon as the EEJ

has recovered, a well developed EIA reappears, which happens about 5 h after the transition event. These observations are consistent with our findings that a weak CEJ is still associated with an eastward electric field.

6. Conclusions

[43] We have investigated the relation between prime parameters of the EIA strength at 400-km altitude, such as the CTR and the crest *L*-value, and the E region eastward electric field based on vertical plasma drift velocities observed at Jicamarca, Peru. Our intention was to verify whether these quantities are significantly correlated, and to compare these results with correlations between the same EIA parameters and the EEJ strength. The study was performed over an almost continuous time span of 5 years, and the sampling is free of local time and seasonal biases. Significant correlation coefficients in all analyses of $cc = 0.8$ or higher confirm that the vertical plasma drift velocity and the EEJ strength are meaningful quantities for describing the emergence of the EIA structure. A preferred response time of the EIA CTR to variations of v_z is 1–2 h, and it is 2–4 h when compared to the EEJ strength. We explain the delayed response to the EEJ strength by the additional information on plasma density carried in the EEJ measurements. This information is absent in the direct estimates of the electric field driving v_z.

[44] The paper provides quantitative expressions for the EIA strength at 400-km altitude which can be expected 2 h after the observation of the electric field proxies in the Peruvian sector. The presented relations can be used in practical applications for estimating the intensity of the EIA during daytime. When the EEJ strength is applied as the proxy, it should be noted that an EIA can even develop for weak CEJ. By direct correlation between the v_z and the EEJ strength a bias vertical drift velocity of $\sim$8 m/s corresponding to an eastward electric field of $\sim$0.2 mV/m was found.

[45] We should point out that equations (4)–(9) present a first order approximation based on the most important ingredient for EIA formation, the electric field. This analysis does not consider the modulating effect of the neutral winds. Meridional winds undergo seasonal variation and they are contributing to the asymmetry of the crest magnitudes [*Rishbeth*, 1972]. Since we are presenting multiyear averages, our study does not consider the EIA asymmetry, but the mean EIA strength at 400-km altitude. In that respect we present the seasonal average of the relations between the electric field and the EIA.

[46] Because of limited data availability, the quantitative relations have been retrieved only for medium to low solar flux conditions of $P < 130$. Although we have no indication that significantly different values are expected in equations (4)–(9) for higher *P*-ranges, the relation should be further investigated during the upcoming solar maximum.

[47] **Acknowledgments.** We would like to thank B. Fejer for helpful discussions on the subject. The CHAMP mission is supported by the German Aerospace Center (DLR) in operation and by the Federal Ministry of Education (BMBF), as part of the Geotechnology Program, in data processing. The operation of the JULIA radar and provision of data by the Jicamarca observatory is gratefully acknowledged.

[48] Amitava Bhattacharjee thanks the reviewers for their assistance in evaluating this paper.

References

Abdu, M. A., G. O. Walker, B. M. Reddy, J. H. A. Sobral, B. G. Fejer, T. Kikuchi, N. B. Trivedi, and E. P. Szuszczewicz (1990), Electric field versus neutral wind control of the equatorial anomaly under quiet and disturbed condition: A global perspective from SUNDIAL 86, *Ann. Geophys.*, *8*, 419–430.

Anderson, D. N. (1981), Modeling the ambient, low latitude *F*-region ionosphere—A review, *J. Atmos. Terr. Phys.*, *43*, 753–762.

Anderson, D., A. Anghel, Y. Yumoto Kiyohumi, M. Ishitsuka, and E. Kudeki (2002), Estimating daytime vertical $E \times B$ drift velocities in the equatorial *F*-region using ground-based magnetometer observations, *Geophys. Res. Lett.*, *29*(12), 1596, doi:10.1029/2001GL014562.

Appleton, E. V. (1954), The anomalous equatorial belt in the F2-layer, *J. Atmos. Terr. Phys.*, *5*, 348.

Bilitza, D. (1990), International Reference Ionosphere 1990, *Tech. Rep. 90-22*, NSSDC/WDC-A-R&S, Greenbelt, MD.

Chau, J. L., and R. F. Woodman (2004), Daytime vertical and zonal velocities from 150-km echos: Their relevance to *F*-region dynamics, *Geophys. Res. Lett.*, *31*, L17801, doi:10.1029/2004GL020800.

Deshpande, M. R., et. al (1977), Effect of electrojet on the TEC of the ionosphere over India subcontinent, *Nature*, *265*, 599.

Duncan, R. A. (1959), The equatorial *F*-region of the ionosphere, *J. Atmos. Terr. Phys.*, *18*, 89–100.

Dunford, E. (1967), The relationship between the ionospheric equatorial anomaly and the *E*-region current system, *J. Atmos. Terr. Phys.*, *29*, 1489–1498.

Dunford, E. (1970), Electric fields and *F*-region electron density over Peru, *J. Atmos. Terr. Phys.*, *32*, 421–425.

Fejer, B. G., E. R. de Paula, R. A. Heelis, and W. B. Hanson (1995), Global equatorial ionospheric vertical plasma drifts measured by the AE-E satellite, *J. Geophys. Res.*, *100*, 5769–5776.

Gouin, P., and P. N. Mayaud (1967), A propos de l'existence possible d'un contre électrojet aux latitudes magnétiques équatoriales, *Ann. Geophys.*, *23*, 41–47.

Heelis, R. A. (2004), Electrodynamics in the low and middle latitude ionosphere: A tutorial, *J. Atmos. Sol.-Terr. Phys.*, *66*, 825–838, doi:10.1016/j.jastp.2004.01.034.

Huang, Y.-N., K. Cheng, and S.-W. Chen (1989), On the equatorial anomaly of the ionospheric total electron content near the Northern Anomaly Crest Region, *J. Geophys. Res.*, *94*, 13,515–13,525.

Hysell, D. L., M. F. Larsen, and R. F. Woodman (1997), JULIA radar studies of electric fields in the equatorial electrojet, *Geophys. Res. Lett.*, *24*, 1687–1690.

Kelley, M. C. (1989), *The Earth's Ionosphere: Plasma Physics and Electrodynamic*, Academic, San Diego.

Kudeki, E., and C. D. Fawcett (1993), High Resolution observations of 150 km echos at Jicamarca, *Geophys. Res. Lett.*, *20*, 1987–1990.

Liu, H., C. Stolle, M. Förster, and S. Watanabe (2007), Solar activity dependence of the electron density at 400 km at equatorial and low latitudes observed by CHAMP, *J. Geophys. Res.*, *112*, A11311, doi:10.1029/2007JA012616.

Lühr, H., S. Maus, and M. Rother (2004), Noon-time equatorial electrojet: Its spatial features as determined by the CHAMP satellite, *J. Geophys. Res.*, *109*, A01306, doi:10.1029/2002JA009656.

Manoj, C., H. Lühr, S. Maus, and N. Nagarajan (2006), Evidence for short spatial correlation lengths of the noontime equatorial electrojet inferred from a comparison of satellite and ground magnetic data, *J. Geophys. Res.*, *111*, A11312, doi:10.1029/2006JA011855.

McNamara, L. F., D. L. Cooke, C. E. Valladares, and B. W. Reinisch (2007), Comparison of CHAMP and Digisonde plasma frequencies at Jicamarca, Peru, *Radio Sci.*, *42*, RS2005, doi:10.1029/2006RS003491.

Mendillo, M., L. Bosheng, and J. Aarons (2000), The application of GPS observations to equatorial aeronomy, *Radio Sci.*, *35*, 885–904.

Millward, G. H., I. C. F. Müller-Wodarg, A. D. Aylward, T. J. Fuller-Rowell, A. D. Richmond, and R. J. Moffett (2001), An investigation into the influence of tidal forcing on *F* region equatorial vertical ion drift using a global ionosphere-thermosphere model with coupled electrodynamics, *J. Geophys. Res.*, *106*, 24,733–24,744.

Murphy, J. A., and R. A. Heelis (1986), Implications of the relationship between electromagnetic drift components at mid and low latitudes, *Planet. Space Sci.*, *34*, 645–652.

Namgaladze, A. A., Y. N. Korenko, V. V. Klimenko, I. V. Karpov, V. A. Surotkin, and N. M. Naumova (1991), Numerical modelling of the thermosphere-ionosphere-protonosphere system, *J. Atmos. Sol.-Terr. Phys.*, *58*, 1113–1124.

Pingree, J. E., and B. G. Fejer (1987), On the height variation of the equatorial *F* region vertical plasma drift, *J. Geophys. Res.*, *92*, 4763–4766.

Prölss, G. W. (2005), *Physics of the Earth's Space Environment*, Springer, Berlin.

Rama Rao, P. V. S., S. Gopi Krishna, K. Niranjan, and D. S. V. V. D. Prasad (2006), Temporal and spatial variations in TEC using simultaneous measurements from the Indian GPS network of receivers during the low solar activity period of 2005–2005, *Ann. Geophys.*, *24*, 3279–3292.

Rastogi, R. G. (1974), Westward equatorial electrojet during daytime hours, *J. Geophys. Res.*, *79*(10), 1203–1512.

Rastogi, R. G., and J. A. Klobuchar (1990), Ionospheric electron content within the equatorial F_2 layer anomaly belt, *J. Geophys. Res.*, *95*, 19,045–19,052.

Reigber, C., H. Lühr, and P. Schwintzer (2002), CHAMP mission status, *Adv. Space Res.*, *30*, 129–134.

Richmond, A. D., E. C. Ridley, and R. G. Roble (1992), A magnetosphere-thermosphere-ionosphere-electrodynamic general circulation model, *J. Geophys. Res.*, *103*, 17,467.

Rishbeth, H. (1972), Thermospheric winds and the *F*-region: A review, *J. Atmos. Terr. Phys.*, *34*, 1–47.

Scherliess, L., and B. G. Fejer (1997), Storm time dependence of equatorial disturbance dynamo zonal electric fields, *J. Geophys. Res.*, *102*, 24,037–24,046.

Schunk, R., L. Scherliess, J. Sojka, D. Thompson, and L. Zhu (2005), Ionospheric weather forecasting on the horizon, *Space Weather*, *3*, S08007, doi:10.1029/2004SW000138.

Stenning, R. J. (1992), Modelling the low latitude *F*-region, *J. Atmos. Terr. Phys.*, *54*(11/12), 1387–1412.

Su, Y. Z., K.-I. Oyama, G. J. Bailey, T. Takahashi, and S. Watanabe (1995), Comparison of satellite electron density and temperature measurements at low latitudes with a plasmasphere-ionosphere model, *J. Geophys. Res.*, *100*, 14,591–14,605.

Walker, G. O., J. H. K. Ma, and E. Golton (1994), The equatorial ionospheric anomaly in electron content from solar minimum to solar maximum for South East Asia, *Ann. Geophys.*, *12*, 195–209.

P. Alken, C. Manoj, and S. Maus, CIRES, University of Colorado and NOAA's National Geophysical Data Center, Boulder, CO, USA.

H. Lühr and C. Stolle, GFZ German Research Centre for Geosciences, Section 2.3 Earth Magnetic Field, Telegrafenberg, Potsdam 14473, Germany. (stolle@gfz-potsdam.de)